

## Analysis of Instabilities in Piezoelectric Transformers Driving Cold Cathode Fluorescent Lamps

G. Spiazzi, S. Buso

Department of Information Engineering

University of Padova

Via Gradenigo 6/b, 35131 Padova - ITALY

Phone: +39-049-827.7525 Fax: +39-049-827.7599/7699

e-mail: [simone.buso@dei.unipd.it](mailto:simone.buso@dei.unipd.it), [giorgio.spiazzi@dei.unipd.it](mailto:giorgio.spiazzi@dei.unipd.it)

**Abstract** – This paper analyzes the behavior of power supplies for cold cathode fluorescent lamps (CCFLs) employing piezoelectric transformers (PTs). It has been demonstrated that the non-linear equivalent lamp resistance interacts with the PT, that behaves like a high-Q resonant circuit, giving rise to instabilities in the audible frequency range [11]. Moreover, when the PTs are driven by a voltage-fed inverter and its DC supply voltage is used to control the lamp voltage, the relation between the control variable and the lamp current can become non monotonic, depending also on the coupling network used between the inverter and the PT. This paper extends the analysis reported in [11] by considering different coupling networks as well as considering the inverter switching frequency as the control variable for controlling the lamp current. SPICE simulations and analytical models are employed to explain the unstable behaviors observed in different experimental prototypes.

### KEYWORDS

Piezoelectric transformers, cold cathode fluorescent lamps, lamp ballasts.

### I. INTRODUCTION

The efforts towards low-cost and low profile power supplies for cold cathode fluorescent lamps (CCFLs) have led to the increasing use of piezoelectric transformers (PTs) instead of the more conventional magnetic transformers, mainly for the following advantages [1-5]:

- inherent high gain at no load, that provides the needed lamp ignition voltage, and a load dependent gain that avoids the use of the ballast capacitor in series with the lamp;
- absence of leakage magnetic field;
- sinusoidal lamp current waveform, thanks to their high Q factor, that enhances the linearity between the average rectified lamp current value, that is usually the measured variable, and the true RMS current value, especially during dimming;
- small size and weight;
- high reliability due to the absence of a high voltage secondary winding.

Usually the inverter design for driving PTs takes advantage of their well known linear model (Rosen-type, see [6]), considering a constant load resistance corresponding to the lamp nominal power. However, it has already been demonstrated in [7-11], that the non linear nature of the lamp equivalent resistance can cause unexpected behaviors when used in conjunction with high output impedance drivers and also with PTs. In [11], the PT-CCFL combination has been analyzed considering a constant frequency inverter driving the PT through a series coupling inductor  $L_s$ , employed mainly to achieve soft commutation of the inverter switches [Fig. 1a and b]. In this paper, the analysis is extended by considering different coupling networks [Fig. 1c and d] and taking, as the control variable, the inverter DC supply voltage as well as the inverter switching frequency. The analytical results are well supported by SPICE simulations, using a suitable lamp model, as well as experimental measurements.

### II. CONVERTER DESCRIPTION

The converter structure we are going to analyze is shown in Fig. 1a: a half-bridge voltage-fed inverter produces a square wave voltage  $u_{inv}$  that is coupled to the PT through a suitable coupling network, that is employed to achieve zero-voltage commutations of the inverter switches. The network can consist of different impedance arrangements, as shown in Fig. 1b), c) and d). The well known Rosen-type model is used to describe the PT behavior around its fundamental resonant mode.

The Rosen-type model parameter values of the PT used in the experimental setup are reported in Table I. In the following, the theoretical analysis and all simulations will use these parameter values.

**Table I – Piezoelectric transformer Fuji T2508A: Rosen type model parameter values**

$R = 5.37\Omega$	$C = 10.22\text{nF}$
$C_1 = 150.4\text{nF}$	$C_0 = 15.48\text{pF}$
$L = 0.699\text{mH}$	$n_{21} = 50.749$

Preliminary experimental measurements done using coupling network  $CN_1$ , showed unstable operation modes in open loop conditions, i.e. with no lamp current control. Two different behaviors have been found: a large signal

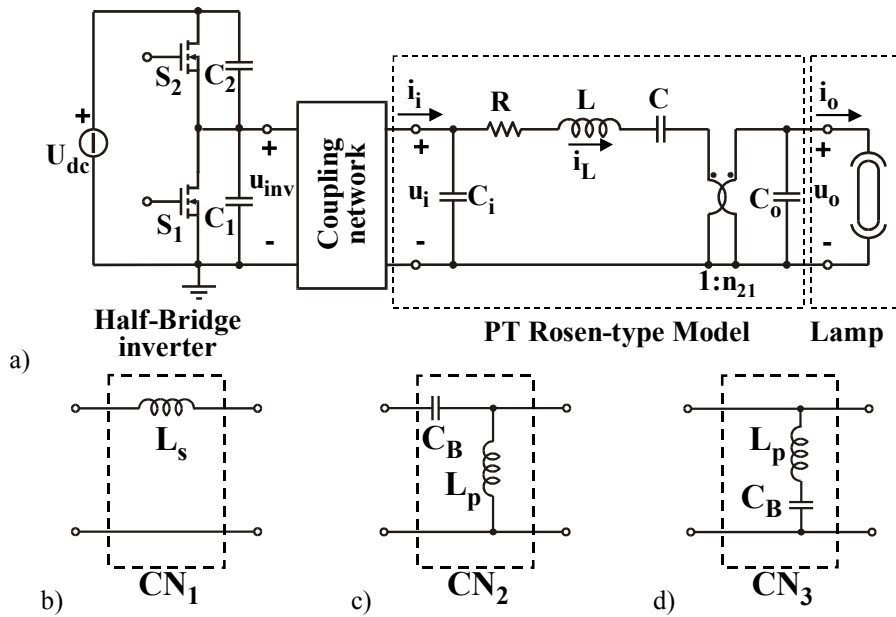


Fig. 1 – a) Scheme of the half-bridge inverter driving the PT for CCFL; b), c) d) different coupling networks.

instability, which makes the lamp behave like a bi-stable circuit and therefore makes the system uncontrollable, and a small signal instability, that makes the electric variables of the system oscillate steadily around their nominal values. Examples of such experimentally found instabilities are shown in Fig. 2 in the case of coupling network CN<sub>1</sub> with  $L_s = 28\mu\text{H}$ ,  $f_{sw} = 65\text{kHz}$ ,  $U_{dc} = 14.7\text{V}$  (upper curve: inverter output current  $i_{Ls}$  [1A/div]; lower curve: PT input voltage  $u_i$  [10V/div]). The measured oscillation frequency is around 6kHz.

In the following section the origin of small-signal and large-signal instabilities is reviewed and a suitable lamp model is considered that allows to verify the observed behavior both analytically and by SPICE simulations.

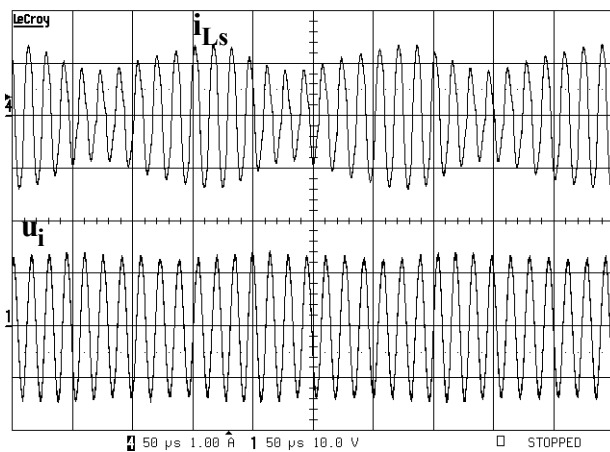


Fig. 2 – Experimental small-signal instability with simple inductor coupling network CN<sub>1</sub> ( $L_s = 28\mu\text{H}$  at  $f_s = 65\text{kHz}$  and  $U_{dc} = 14.7\text{V}$ ). Upper curve: inverter output current  $i_{Ls}$  [1A/div]; lower curve: PT AC input voltage  $u_i$  [10V/div].

### III. REVIEW OF SMALL-SIGNAL AND LARGE-SIGNAL INSTABILITIES

As demonstrated in [7-11], neglecting the non-linear nature of the lamp impedance hides many important phenomena, when PTs are used to drive CCFLs. For this reason, a suitable lamp model must be employed for both analysis and simulations: here the model proposed in [12] has been considered, where the lamp resistance is approximated by an exponential function of the lamp power, i.e.

$$R_L = a e^{-bP_L} \tag{1}$$

where  $a$  and  $b$  are suitable coefficients to be selected based on lamp measurements. The parameters of the CCFL used in the experimental setup are reported in Table II: for this lamp the resistance variation can be reasonably approximated by choosing  $a = 1.6\text{M}\Omega$  and  $b = 0.43\text{W}^{-1}$  in (1).

Lamp Voltage ( $V_{RMS}$ ) 25°C	910	
Starting Voltage (V)	0°C - 25°C	1850 - 1474
Lamp Current ( $\text{mA}_{RMS}$ )	6.0	
Ambient operating range (°C)	-10 to 70	

The large-signal relation (i.e. the steady-state regulation curve) between the lamp current and the control variable (the inverter DC supply voltage  $U_{dc}$  or the inverter switching frequency  $f_{sw}$ ) is calculated in the following way: starting from the desired lamp current value, the lamp voltage is calculated from (1), then from the knowledge of the voltage gain between the fundamental component of the inverter output voltage  $u_{inv}$  and the lamp voltage, that depends on the considered coupling network and on the PT model, the

needed DC voltage  $U_{dc}$  at fixed switching frequency or the needed switching frequency  $f_{sw}$  at fixed DC voltage are calculated. In both cases, a square wave inverter voltage  $u_{inv}$  was considered, which is a good approximation only if the dead time between the half-bridge switches is small compared to the switching period (this is the case when coupling network  $CN_1$  is used). When  $CN_2$  and  $CN_3$  are considered, the inverter voltage looks more like a trapezoidal waveform, but since the aim is to reveal non monotonic control characteristics, the approximation was still considered acceptable.

The same lamp model (1) can be used to analyze the circuit behavior from a small-signal stability point of view. In fact, the negative lamp small-signal resistance would predict an unstable system in any condition, while many combinations PT-CCFL are, indeed, stable. As explained in [7-11], this behavior can be theoretically explained by considering a delay  $\tau_L = 1/\omega_L$  between the lamp power variation and the corresponding equivalent lamp resistance variation, which accounts for the plasma ionization time constant. To this purpose, in the lamp PSPICE model, like that reported in [12], the R-C low-pass filter, that is used to derive the average lamp power so as to calculate the lamp resistance according to (1), also accounts for the aforementioned delay. The simulation performed with  $\omega_L = 150$  krad/s in the same conditions of the measured waveforms in Fig. 2, revealed the same instability, but at a slightly higher oscillation frequency (10kHz), as can be seen in Fig. 3.

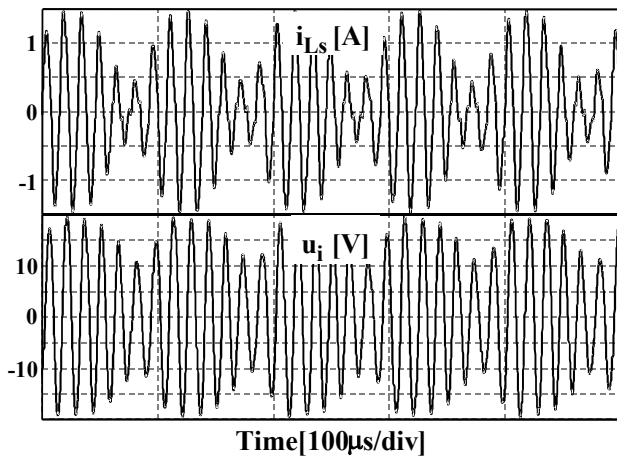


Fig. 3. Simulated Small-signal instability observed with simple inductor coupling network  $CN_1$  with  $\omega_L = 150$  krad/s ( $L_s = 28\mu\text{H}$  at  $f_s = 65\text{kHz}$  and  $U_{dc} = 14.7\text{V}$ ). Upper curve: inverter output current  $i_{Ls}$ ; lower curve: PT AC input voltage  $u_i$ .

The instability occurrence can also be explained by considering the lamp incremental impedance, that can be derived directly from (1) by perturbation under small-signal assumption (see [11]). The result is:

$$Z_L = \frac{\hat{u}_o}{\hat{i}_o} = R_{LN} \left( \frac{\omega_z}{\omega_p} \right) \left( \frac{1 + \frac{s}{\omega_z}}{1 + \frac{s}{\omega_p}} \right), \quad (2)$$

where  $R_{LN} = a e^{-bP_L}$  is the lamp resistance at the considered operating point  $[U_o, I_o]$ ,  $P_L = U_o \cdot I_o$  is the lamp power, and  $\omega_z = \omega_L(1 - bP_L)$ ,  $\omega_p = \omega_L(1 + bP_L)$ . Note that the DC small-signal lamp resistance is negative, since  $\omega_z$  and  $\omega_p$  have opposite signs, while, at high frequency, the RHP zero makes the small-signal lamp resistance positive. This behavior is in agreement with previously developed small-signal lamp models, like those described in [7, 8]. The low-frequency negative resistance can cause instabilities when the lamp is driven by a low-impedance voltage source.

#### IV. COUPLING NETWORK $CN_1$

The series inductor  $L_s$ , is the only coupling network that provides an almost true sinusoidal driving waveform for the PT. Moreover, since the soft-switching condition requires the capability of charging and discharging only the switch output capacitances, a minimum reactive energy is necessary. However, as already stated in many papers, the series inductor introduces a resonance with the PT input capacitance that modifies the overall voltage gain between the RMS value of the inverter output voltage fundamental component and the lamp voltage. Fig. 4 reports different voltage conversion ratios as functions of the switching frequency  $f_{sw}$  taken at two lamp current values ( $L_s = 42\mu\text{H}$ ):  $M_{PT}$  represents the PT intrinsic voltage gain,  $M_i$  is the voltage gain between the RMS value of the inverter voltage fundamental component and the RMS value of the PT input voltage  $U_i$ , and  $M_g = M_i \cdot M_{PT}$  represents the overall voltage gain. It is interesting to note that the presence of the coupling inductor  $L_s$  introduces an additional voltage gain ( $M_i$ ) that is frequency dependent and shows two resonance peaks: one below and the other above the PT resonance peak. These modifications make more problematic the control of the lamp current using the switching frequency as the control parameter, since, moving along the overall voltage conversion ratio curve, the gain (i.e. the curve slope) changes sign many times. However, with a proper choice of the inductance value and of the DC link voltage it is possible to change the lamp current by varying the inverter switching frequency, as shown in Fig. 4, where the two switching frequency values ( $f_1$  and  $f_2$ ) corresponding to  $6\text{mA}_{RMS}$  and  $1\text{mA}_{RMS}$  lamp current values are reported (with  $U_{dc} = 13\text{V}$ ). The chosen coupling inductor value allows to achieve soft switching in any condition (the worst case is the maximum lamp current), as revealed by Fig. 5 that reports magnitude and phase of the overall impedance  $Z_g$  seen by the inverter for two different lamp current values. In both cases, the needed switching frequency falls inside the interval in which the inverter output current lags the inverter output voltage, thus allowing the inductor current to charge and discharge the switch output capacitances during the switch dead time.

The simulated inverter output current and voltage taken at  $I_o = 6\text{mA}_{RMS}$  confirm this result, as revealed by Fig. 6.

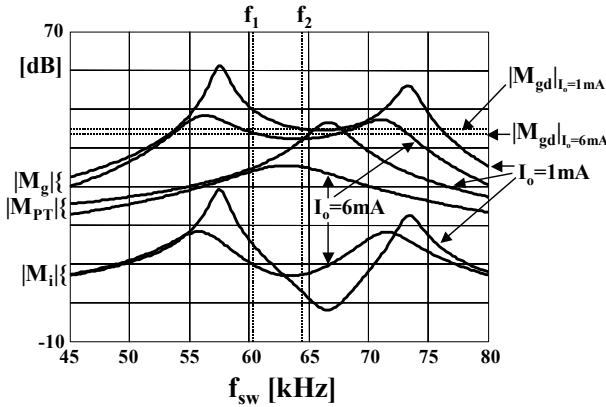


Fig. 4 – Voltage gains for coupling network CN<sub>1</sub> at two different lamp current values ( $L_s = 42\mu\text{H}$ ). The desired overall voltage gains  $M_{gd}$  needed to obtain the given lamp current values with  $U_{dc} = 13\text{V}$  are also reported.

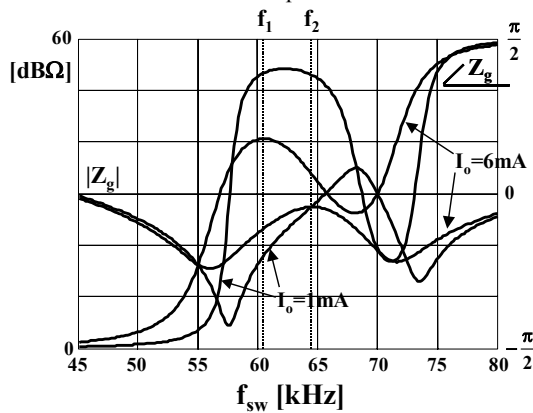


Fig. 5 – Magnitude and phase of the impedance  $Z_g$  seen by the inverter for two different lamp current values.

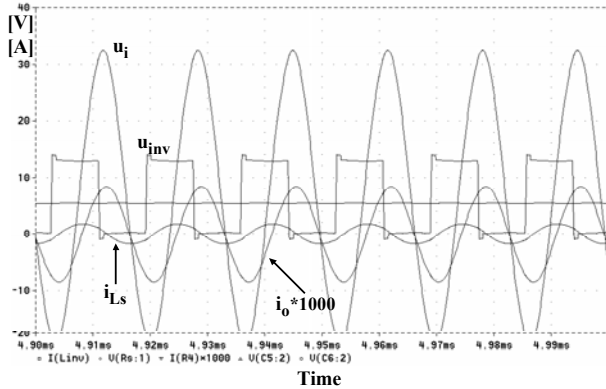


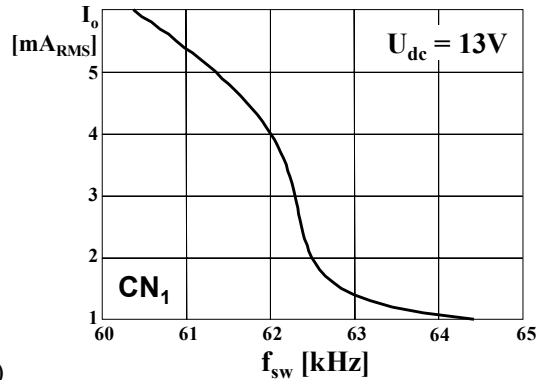
Fig. 6 – Simulated main converter waveforms at  $I_o = 6\text{mA}_{\text{RMS}}$ .

The regulation curve, i.e.  $I_o = f(f_{sw})$ , is reported in Fig. 7a: as can be seen, even using the switching frequency as control parameter the variation of the curve slope reveals a quite varying small-signal DC gain. This behavior becomes much worse when a constant switching frequency operation with a variable DC link voltage  $U_{dc}$  is considered, as revealed by the regulation curve reported in Fig. 7b ( $L_s = 42\mu\text{H}$ ): here, as stated also in [11], a too high coupling inductor value causes the regulation curve to become non monotonic (its slope changes sign), thus making impossible the lamp current control. A regular curve is obtained if a lower  $L_s$  value is used, as shown in Fig. 7b for  $L_s = 38\mu\text{H}$ ,

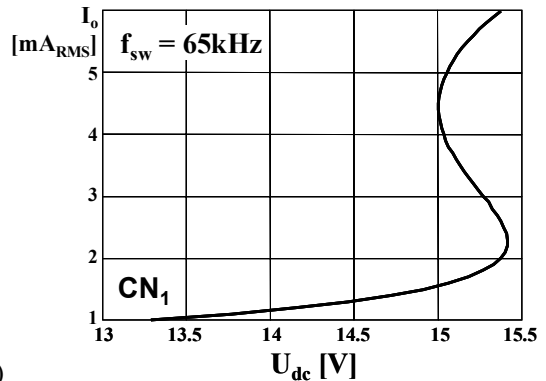
but at the expense of losing the soft-switching condition at nominal load.

The high non linearity in the regulation curve at constant switching frequency was verified by experimental measurements: Fig. 8 reports the main converter waveforms when the DC link voltage is slowly approaching the value at which the regulation curve changes slope: the operating point moves abruptly to a very high lamp current value with a dangerous high PT input voltage value. This snap happens at  $U_{dc} = 21\text{V}$ , a higher value compared to that predicted by theoretical analysis (see Fig. 7b).

As already stated in the previous section, the small-signal behavior does not depend on the chosen control variable, and a small-signal instability can arise, as shown in Fig. 2.



a)



b)

Fig. 7 – Regulation curves with CN<sub>1</sub> ( $L_s = 42\mu\text{H}$ ): a) at constant DC link voltage ( $U_{dc} = 13\text{V}$ ); b) at constant switching frequency ( $f_{sw} = 65\text{kHz}$ ).

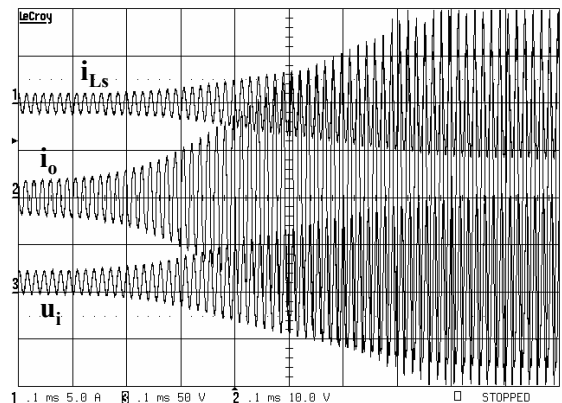


Fig. 8 – Main converter waveforms when  $U_{dc}$  is slowly approaching 21V ( $f_{sw} = 65\text{kHz}$ ,  $L_s = 42\mu\text{H}$ ). From top to bottom: inductor current  $i_{Ls}$  [5A/div], lamp current  $i_o$  [10mA/div], PT input voltage  $u_i$  [50V/div].

V. COUPLING NETWORK CN<sub>2</sub> AND CN<sub>3</sub>

The other two coupling networks in Fig. 1, that use a parallel inductor  $L_p$ , behave quite similarly, since they differ only for the position of the DC blocking capacitor  $C_B$ . For this reason, the analysis reported in the following refers to CN<sub>2</sub>, the analysis with CN<sub>3</sub> giving the same results. CN<sub>2</sub> has the advantage of eliminating the DC component from the PT input voltage, which reduces its driving RMS voltage, but slightly modifies the overall voltage gain as shown in Fig. 9, that reports the voltage gains for two different lamp current values ( $C_B = 1\mu F$ ,  $L_p = 20\mu H$ ). For a constant  $U_{dc}$  voltage of 30V, the same figure shows the overall voltage gains  $M_{gd}$  needed to obtain the desired lamp current values, and the corresponding switching frequencies  $f_1$  and  $f_2$ . As already stated in [5], the parallel inductor arrangement can always allow to achieve soft commutations of the inverter switches if a sufficiently high reactive current is absorbed by the inductor. This is also revealed by the plot of the phase of the impedance  $Z_g$  seen by the inverter, shown in Fig. 10: with a constant DC link voltage, the inverter operates at switching frequency  $f_1$  for  $I_o = 6mA$ , and at  $f_2$  for  $I_o = 1mA$ . In both cases the inverter output current will be lagging the inverter output voltage. However, differently from the previous case, now the inductor current  $i_{Lp}$  has to charge and discharge also the PZT input capacitance, that is much higher than the switch output capacitances, so that the positive impedance phase is a necessary but not sufficient condition to achieve soft commutations. Fig. 11, shows experimental waveforms taken at  $f_{sw} = 65kHz$  and  $U_{dc} = 20V$ : as can be seen, the inverter switches must have enough dead time to allow charging and discharging of the overall output capacitance, giving rise to a trapezoidal output voltage waveform.

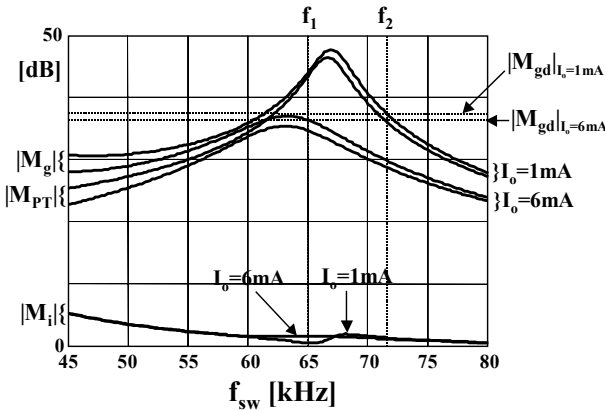


Fig. 9 – Voltage gains for coupling network CN<sub>2</sub> at two different lamp current values ( $C_B = 1\mu F$ ,  $L_p = 20\mu H$ ). The desired overall voltage gains  $M_{gd}$  needed to obtain the given lamp current values with  $U_{dc} = 30V$  are also reported.

Similarly to the case of CN<sub>1</sub>, also with CN<sub>2</sub> a sufficiently low lamp delay causes the system to become unstable. This behavior is confirmed by both PSPICE simulation and by experimental measurements: Fig. 12 reports the inductor current  $i_{Lp}$  and the lamp current  $i_o$  measured at  $U_{dc} = 15V$  and  $f_{sw} = 65kHz$ , revealing an oscillation around the operating point at  $f_{osc} = 6.5kHz$ . The same analysis done with coupling network CN<sub>3</sub> reveals a similar behavior:

clearly the small-signal instability is mainly related to the interaction between the lamp and the PT and is almost independent of the used coupling network.

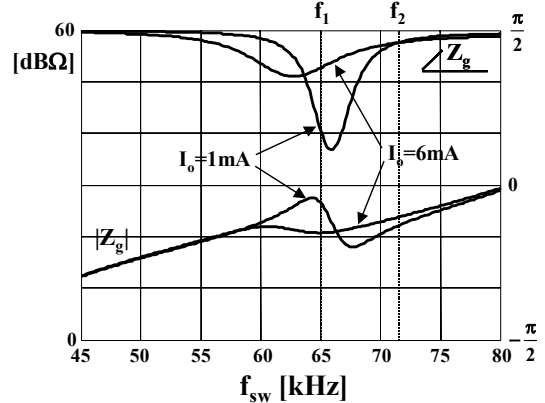


Fig. 10 – Magnitude and phase of the impedance  $Z_g$  seen by the inverter for two different lamp current values.

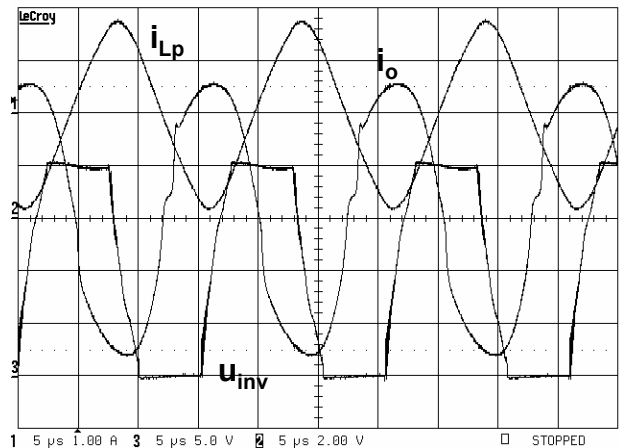


Fig. 11 – Experimental waveforms with coupling network CN<sub>2</sub> ( $L_p = 20\mu H$ ,  $C_B = 1\mu F$ , at  $f_s = 65kHz$  and  $U_{dc} = 20V$ ). Upper curve: inductor current  $i_{Lp}$  [1A/div]; center curve: lamp current  $i_o$  [2mA/div]; lower curve: inverter output voltage  $u_{inv}$  [5V/div].

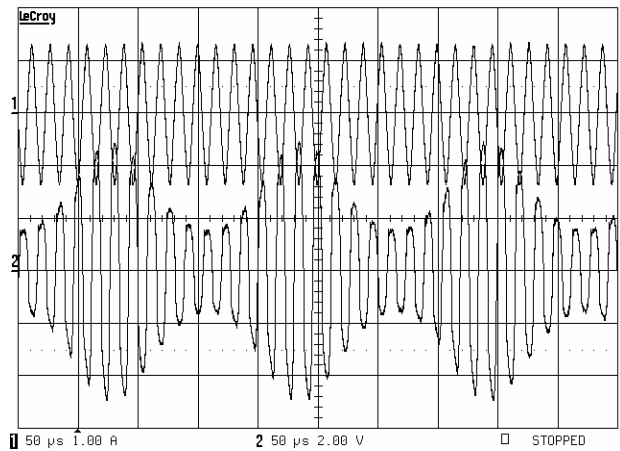


Fig. 12 - Small-signal instability observed with CN<sub>2</sub> at  $f_s = 65kHz$  and  $U_{dc} = 15V$ . Upper curve: inductor current  $i_{Lp}$  [1A/div]; lower curve: lamp current  $i_o$  [2mA/div].

Now we want to investigate the large signal behavior when the DC link voltage is varied at constant switching frequency or when the switching frequency is used as control variable at constant DC link voltage. In the first case, the regulation curve  $I_o = f(U_{dc})$  is shown in Fig. 13a, while the regulation curve  $I_o = f(f_{sw})$  is shown in Fig. 13b: in both cases a regular behavior is observed, that holds for different coupling network parameter values. Similar results are obtained with CN<sub>3</sub>. From this point of view, the coupling network with parallel inductor gives less control problems than the series inductor.

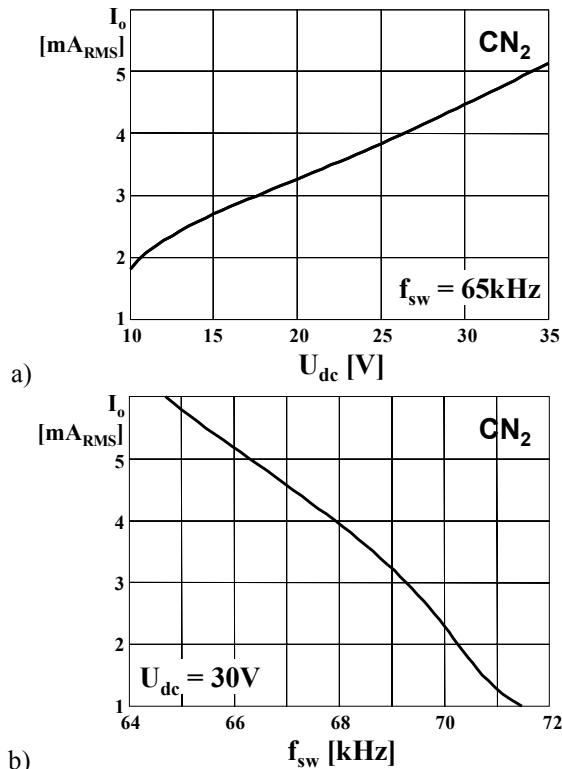


Fig. 13 – Regulation curves with CN<sub>2</sub> ( $L_p = 20\mu\text{H}$ ,  $C_B = 1\mu\text{F}$ ). a) At constant switching frequency ( $f_s = 65\text{kHz}$ ); b) at constant DC link voltage ( $U_{dc} = 30\text{V}$ ).

## VI. CONCLUSIONS

The negative incremental lamp impedance of a cold cathode fluorescent lamp can cause instabilities when the lamp is driven by a piezoelectric transformer. Such instabilities depend mainly on the PT parameters and lamp characteristics, and only to less extent on the coupling network usually employed between the inverter and the PT in order to achieve soft commutation of the inverter switches. These coupling networks can also cause a strong non linear regulation curve between the control variable (either the inverter DC link voltage or switching frequency), that can, in the case of CN<sub>1</sub>, preclude a correct lamp current control. SPICE simulations and analytical models have been employed to justify the behaviors observed in different experimental measurements.

## VII. REFERENCES

- [1] Ray L. Lin, Fred C. Lee, Eric M. Baker and Dan Y. Chen, "Inductorless Piezoelectric Transformer Electronic Ballast for Linear Fluorescent Lamp" IEEE Applied Power Electronic Conference Proc (APEC), 2001, pp.664-669.
- [2] Chin S. Moo, Wei M. Chen, Hsien K. Hsieh, "An Electronic Ballast with Piezoelectric transformer for Cold Cathode Fluorescent Lamps" Proceedings of IEEE International Symposium on Industrial Electronics (ISIE), 2001, pp. 36-41.
- [3] H. Kakehashi, T. Hidaka, T. Ninomiya, M. Shoyama, H. Ogasawara, Y. Ohta, "Electronic Ballast using Piezoelectric transformer for Fluorescent Lamps" IEEE Power Electronics Specialists Conference Proc. (PESC), 1998, pp.29-35.
- [4] Sung-Jim, Kyu-Chan Lee and Bo H. Cho, "Design of Fluorescent Lamp Ballast with PFC using Power Piezoelectric Transformer" IEEE Applied Power Electronic Conference Proc. (APEC), 1998, pp.1135-1141.
- [5] M. Sanz, P. Alou, R. Prieto, J. A. Cobos and J. Uceda, "Comparison of different alternatives to drive Piezoelectric Transformers" IEEE Power Electronics Specialists Conference, PESC'02, Proceedings pp.358-364, 2002.
- [6] Ray L. Lin, Eric Baker and Fred C. Lee, "Characterization of Piezoelectric Transformers", Proceedings of Power Electronics Seminars at Virginia Tech, Sept. 19-21, 1999, pp. 219-225.
- [7] E. Deng, S. Cuk, "Negative Incremental Impedance and Stability of Fluorescent Lamps," IEEE Applied Power Electronics Conf. Proc. (APEC), 1997. pp.1050-1056.
- [8] S. Ben-Yaakov, M. Shvartsas, S. Glozman, "Statics and Dynamics of Fluorescent lamps Operating at High Frequency: Modeling and Simulation," IEEE Trans. On Industry Applications, vol.38, No.6, Nov./Dec. 2002, pp.1486-1492.
- [9] S. Glozman, S. Ben-Yaakov, "Dynamic interaction analysis of HF ballasts and fluorescent lamps based on envelope simulation," IEEE Trans. Industry Application, vol. 37, Sept./Oct. 2001, pp. 1531-1536.
- [10] Y. Yin, R. Zane, J. Glaser, R. W. Erickson, "Small-Signal Analysis of Frequency-Controlled Electronic Ballast", IEEE Trans. On Circuits and Systems – I: Fund. Theory and Applications, vol.50, No.8, August 2003, pp.1103-1110.
- [11] G. Spiazzi, S. Buso, "Analysis of Large-Signal and Small-Signal Instabilities in Piezoelectric Transformers Driving Cold Cathode Fluorescent Lamps," IEEE Applied Power Electronics Conf. CDRom (APEC), February, 2004.
- [12] M. Cervi, A. R. Seidel, F. E. Bisogno, R. N. do Prado, "Fluorescent Lamp Model Based on the Equivalent Resistance Variation," IEEE Industry of Application Society (IAS) CDRom, 2002.